Effective Tensile Strength of Lightly Cemented Sand

Louis Ge, M.ASCE[1]; Yu-Wei Hwang[2]; Hemei Sun[3]; Guan-De He[4]; Renpeng Chen, M.ASCE[5]; and Xin Kang, A.M.ASCE[6]

Abstract: An indentation test was developed to indirectly determine the effective tensile strength of lightly cemented sand by iterative method. The description of the test is followed by a discussion and comparison of the determination of the effective tensile strength of soil under a framework proposed in previous research. Test results reveal that, in general, tensile strength is proportional to indenter diameter (a) to specimen diameter ratio (b), a/b, and has no apparent relationship with the specimen height (H) to diameter ratio, $H/2b$. The iterative method provides a more realistic approach to compute the tensile stress beyond the traditional method. In addition, the iterated parameter, K, was found to be linearly related to the a/b ratio, for a given specimen, regardless of $H/2b$ value. Finally, the effective tensile strength was verified by an indentation test in conjunction with the pressure plate test and consolidated undrained triaxial test under an unsaturated soil framework. **DOI: 10.1061/(ASCE)MT.1943-5533.0002570.** *© 2018 American Society of Civil Engineers.*

Author keywords: Effective tensile strength; Indentation test; Suction stress; Unsaturated soil.

Downloaded from ascelibrary.org by HUNAN UNIVERSITY on 03/20/19. Copyright ASCE. For personal use only; all rights reserved.

Introduction

Tensile strength of soil is normally considered insignificant in geotechnical engineering practice. The relatively small value and immature techniques of tensile strength testing have led to tensile strength being not fully developed in the past. However, the tensile strength of soil can play an important role in engineering design, including slope stability analysis, landslide and tensile crack analysis, pavement, dams, embankments, and other geotechnical structures.

The tensile strength of soil can be determined directly or indirectly. In direct methods, a specimen is directly subjected to tensile forces and being pulled apart in the middle of the specimen (Das and Dass 1995; Nahlawi and Chakrabarti 2004; Tamrakar et al. 2007; Tang and Graham 2000). The tensile strength of soil can be directly computed by dividing the measured maximum tensile force by the cross-sectional area of the splitting plane. However, specimen clamping, surface roughness, and the difficulty of controlling the failure plane can influence the accuracy and consistency of tensile strength measurement. For the indirect methods, on the other hand, the failure plane is not induced by tensile force, where the common test methods include the Brazilian disk test, split tensile test, three-point bending test, four-point bending test, and indentation test. Among these methods, the three-point bending test and four-point bending test are seldom used in soil, while the indentation test has been commonly used. In the indentation test, the tensile strength of soil is computed by equations developed from an associated theory. The indentation test, also called the unconfined penetration test, uses a pair of cylindrical metal indenters to penetrate into a cylindrical specimen (Chen 1969; Fang and Chen 1972; Fang and Fernandez 1981; Kim et al. 2007, 2012). The tensile strength obtained from the indentation test was derived from the limit analysis theory (Chen 1969, 1975).

For soil under neither completely dry nor fully saturated conditions, the matric suction, pertinent to the soil-water characteristic curve (SWCC), has an impact on the tensile strength of soil. The effective tensile strength, which is different from the total tensile strength measured by the indentation test, can truly represent the effective uniaxial tensile strength for their similar failure mode of a soil specimen. Therefore, Lu's unsaturated soil mechanics framework was adopted to compute the effective tensile strength of soils in this study (Lu and Likos 2006; Lu et al. 2009; Oh et al. 2012).

In this paper, the tensile strength of lightly cemented sand was experimentally determined by indentation test. The method is presented and discussed, where an iterative method for determining the K value was developed and verified. Then, the effective tensile strength of the indentation test is computed by employing the concept of suction stress (Lu and Likos 2006). Finally, in conjunction with the Mohr-Coulomb failure envelope, the validity of effective stress principle of unsaturated soils proposed by Lu and Likos (2006), Lu et al. (2009), and Oh et al. (2012) is examined.

Background

Indentation test results are influenced by the size of the specimen and the indenter, degree of saturation of the specimen, and the loading rate. Many researchers have investigated the influence of size variation of indenters and specimens, as well as the plasticity index and water content of soil material, on the results of the indentation test (Chen 1969; Fang and Chen 1972; Fang and Fernandez 1981; Kim et al. 2007, 2012). The tensile strength increases with the

[1]Professor, Dept. of Civil Engineering, National Taiwan Univ., Taipei 10466, Taiwan. Email: louisge@ntu.edu.tw

[2]Research Assistant, National Center for Research on Earthquake Engineering, Roosevelt St., Taipei 10466, Taiwan. Email: yuwei0418@gmail.com

[3]Graduate Student, Dept. of Geotechnical Engineering, College of Civil Engineering, Hunan Univ., Changsha 40010, China. Email: sunhemei@hnu.edu.cn

[4]Formerly, Graduate Student, Dept. of Civil Engineering, National Taiwan Univ., Taipei 10466, Taiwan.

[5]Professor, Dept. of Geotechnical Engineering, College of Civil Engineering, Hunan Univ., Changsha 40010, China. Email: chenrp@hnu.edu.cn

[6]Professor, Dept. of Geotechnical Engineering, College of Civil Engineering, Hunan Univ., Changsha 40010, China (corresponding author). Email: kangxin@hnu.edu.cn

Note. This manuscript was submitted on January 17, 2018; approved on July 17, 2018; published online on October 31, 2018. Discussion period open until March 31, 2019; separate discussions must be submitted for individual papers. This paper is part of the ***Journal of Materials in Civil Engineering***, © ASCE, ISSN 0899-1561.

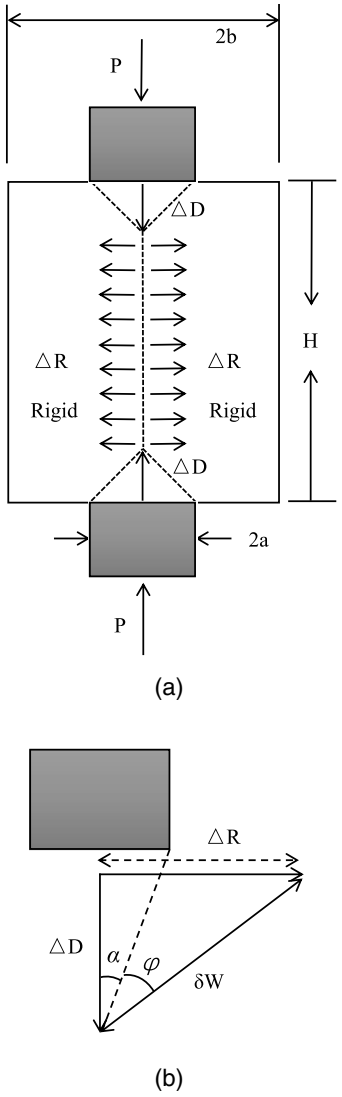

Fig. 1. Limit analysis of indentation test: (a) failure mode of specimen; and (b) vector field of displacement.

increase in diameter of the indenter but decreases with the loading rate. The ratio of specimen height to diameter controls the testing results of tensile strength by employing limit analysis. Fang and Fernandez (1981) concluded that the main parameters will be water content when plasticity index is greater than 20; otherwise, both plasticity and water content play an important role in tensile strength.

Chen postulated a limit analysis model to describe a split tensile failure of a brittle material, as shown in Fig. 1 (Chen 1969). By equating the external work to the internal splitting work, an upper-bound solution can be defined as follows:

$$\frac{P^u}{\pi a^2} = \frac{1-\sin\phi}{2\sin\alpha\cos(\alpha+\phi)}\frac{\sigma^u}{2} + \tan(\alpha+\phi)\left(\frac{bH}{2}-\cot\alpha\right)\sigma^t \quad (1)$$

where P^u is the axial compressive load that causes the splitting failure; a is the radius of the indenter; b is the radius of the specimen; ϕ is the internal friction angle of the soil; α is the developed failure cone angle underneath the indenter when failure occurs; H is the length of the specimen; σ^u is the unconfined compressive strength; and σ^t is the tensile strength that is determined by the indentation test. When $dP^u/d\alpha = 0$, it gives the minimum P^u, where

$$\frac{P^u}{\pi a^2} = \left[\frac{bH}{a^2}\tan(2\alpha+\phi) - 1\right]\sigma^t \quad (2)$$

By combining Eqs. (1) and (2), one gets

$$\cot\alpha = \tan\alpha + \sec\phi\left[1 + \frac{\frac{bH\cos\phi}{a^2}}{\frac{\sigma^u}{\sigma^t}\left(\frac{1-\sin\phi}{2}\right) - \sin\phi}\right]^{\frac{1}{2}} \quad (3)$$

Substituting α from Eq. (3) into Eq. (1), the maximum compressive axial load P will be less than P^u during the test

$$P \le P^u = \pi[bH\tan(2\alpha+\phi) - a^2]\sigma^t \quad (4)$$

$$\sigma^t = \frac{P}{\pi(bHK - a^2)} \quad (5)$$

where $K = \tan(2\alpha+\phi)$, which is a function of internal friction angle, brittleness (unconfined compressive strength to tensile strength ratio, σ^u/σ^t), and the size of the specimen and indenter.

Chen summarized that the upper-bound solution of the limit analysis obtained is close to the real value, and this leads to the use of a constant K value (Chen 1969). Chen also assumed several basic material properties for tensile strength analysis of soils in recent years.

For all soil types, K is assumed to be 1 (Fang and Chen 1972), and Eq. (5) can be rewritten as

$$\sigma^t = \frac{P}{\pi(bH - a^2)} \quad (6)$$

Chen and Fang generalized the values of K for different types of experimental materials with different molds and specimen ratios (Chen 1975; Fang and Chen 1972; Fang and Fernandez 1981). In fact, the constant K value leads to a simple data reduction and can reduce the size effects of the tests. However, it may not truly reflect the brittleness of the tested materials. In this study, the iterative method is used to determine a reasonable K value for calculating the tensile strength, otherwise assumed to be 1 in the past. With the information of the peak axial force P, unconfined compressive strength σ^u, internal friction angle ϕ, and an assumed experimental value for K, a control value for K was calculated directly using Eqs. (3) and (5). When the difference between the experimental value and the control value converges to the minimum condition, the iterated K value was obtained and the tensile strength σ^t can be determined. This study will discuss the size variation of the specimen and indenter, and an iterative method for calculating the tensile strength.

In Terzaghi's principle of effective stress, the effective stress σ' is equal to the total stress σ subtracting the associated pore water pressure u_w

$$\sigma' = \sigma - u_w \quad (7)$$

The equation is appropriate for describing saturated soil; however, it cannot correctly represent the effective stress for the unsaturated soil due to the existence of suction stress. Bishop (1959) attempted to describe the mechanical behavior of unsaturated soil. In partially saturated soils, Bishop modified Terzaghi's equation, including the effect of matric suction, as

$$\sigma' = \sigma - u_a + \chi(u_a - u_w) \quad (8)$$

where u_a is the pore-air pressure, u_w is the pore-water pressure; and χ is the effective stress parameter as a function of degree of saturation. $(\sigma - u_a)$ represents the net normal stress, and $(u_a - u_w)$ is

Downloaded from ascelibrary.org by HUNAN UNIVERSITY on 03/20/19. Copyright ASCE. For personal use only; all rights reserved.

the matric suction. Parameter χ the degree of saturation of the soil and how it makes the matric suction contribute to the effective stress, varying between 0 and 1. Within this framework, Bishop introduced the modified effective stress into the Mohr-Coulomb criterion

$$\tau_f = c' + [\sigma - u_a + \chi(u_a - u_w)] \tan \phi' \tag{9}$$

where c' is effective cohesion and ϕ' is effective angle of friction.

On the other hand, Fredlund and Morgenstern (1977) regarded the boundary between the air and water phase as not homogeneous, and referred to the interface as the contractile skin. The pressure difference in the interface $(u_a - u_w)$ is called the matric suction. Fredlund considered the matric suction as an independent stress-state variable, where the soil particle and contractile skin can reach mechanical equilibrium, and the air or water phase can flow due to the applied pressure. The Mohr-Coulomb failure criterion under Fredlund's framework is given as follows:

$$\tau_f = c' + (\sigma - u_a) \tan \phi' + (u_a - u_w) \tan \phi^b \tag{10}$$

where ϕ^b is an additional friction angle that increases the shear strength of the unsaturated soil due to the matric suction.

Lu and Likos proposed the concept of suction stress to describe the effective stress of unsaturated soil (Lu and Likos 2006; Lu et al. 2009; Oh et al. 2012). In their framework, the particle-scale forces are conceptualized in the following three types: (1) active skeletal force propagated through the soil grains arising from external force (Type I); (2) active local forces concentrated at or near the inter-particle contacts, including van der Waals forces, electrical double-layer forces, cementation forces, surface tension forces, as well as the force arising from negative pore-water pressure—these forces can be conceptually combined into a macroscopic stress called suction stress (Type II); and (3) passive particle-particle contact force serving as counterbalancing force (Type III). Consideration of only Types I and III is often sufficient for saturated soil as captured in Terzaghi's classic effective stress equation in which σ' serves as the Type III force and $(\sigma - u_w)$ represents the Type I force. However, for unsaturated conditions, distinguishing between these three types of forces becomes necessary because the pore pressure disintegrates into several microscopic interparticle forces, which are the major contributors to the tensile strength of soil (Lu and Likos 2006; Lu et al. 2009; Kang et al. 2016b).

Under the framework, the effective stress of unsaturated soil is defined as follows

$$\sigma' = (\sigma - u_a) - \sigma_s \tag{11}$$

where σ' is the effective stress of the unsaturated soil (Type III); u_a is the pore-air pressure; $(\sigma - u_a)$ represents the net normal stress or total stress of the unsaturated soil (Type I); and σ_s is the suction stress (Type II).

On the macroscopic force level, the suction stress σ_s is defined as a combination of matric suction and osmotic suction. Due to the fact that the magnitude of matric suction is generally much larger than osmotic suction, only the matric suction and the degree of saturation are included in formulating the suction stress for the unsaturated soil (Oh et al. 2012)

$$\sigma_s = -S_e(u_a - u_w) \tag{12}$$

where S_e is the equivalent degree of saturation and $(u_a - u_w)$ is matric suction. In establishing an analytical form of the suction stress, the closed-form equation of Genuchten (1980) is used

$$S_e = \left\{ \frac{1}{1 + [\beta(u_a - u_w)^n]} \right\}^{1-\frac{1}{n}} \tag{13}$$

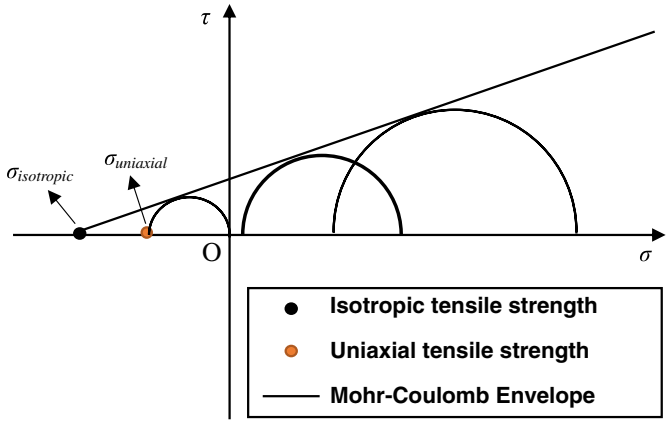

Fig. 2. Unsaturated soil mechanics framework.

where β is the reciprocal of the air-entry pressure and n is the por- size spectrum number. By substituting Eq. (13) into Eq. (12), the following equation defines the relationship between the suction stress and the equivalent effective degree of saturation, S_e:

$$\sigma_s = -\frac{S_e}{\beta}\left(S_e^{\frac{n}{1-n}} - 1\right)^{\frac{1}{n}} \tag{14}$$

This study adopted Lu's concept of effective tensile strength in an unsaturated framework, which is similar to the effective stress principle of Terzaghi. The tensile strength obtained by the indentation test was total strength, so the effective tensile strength should be computed as the total strength minus the suction stress in the unsaturated framework.

In formulating the tensile strength of unsaturated soils, Lu et al. (2009) made a linear extrapolation of the Mohr-Coulomb failure envelope to the zone of tensile normal stress. The interception at the horizontal axis is the isotropic tensile strength, denoted as $\sigma_{t,iso}$ in Fig. 2. The uniaxial tensile strength, $\sigma_{t,uni}$, represents a soil element failing when the tensile stress is acting on one principal plane and no stress on the orthogonal principal planes.

Under the framework of Lu et al., the suction stress needs to be considered when the unsaturated soil condition is simulated through the results of saturated conditions, as depicted in Fig. 3 and as defined in Eq. (15):

$$\sigma_c' = \sigma_s - \sigma_c \tag{15}$$

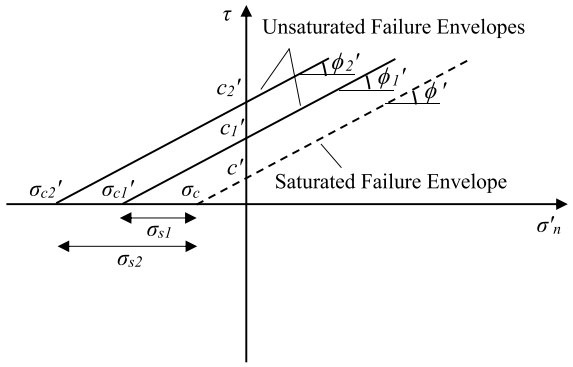

Fig. 3. Relationship of failure envelopes between saturated state and unsaturated state.

Downloaded from ascelibrary.org by HUNAN UNIVERSITY on 03/20/19. Copyright ASCE. For personal use only; all rights reserved.

where σ_c' is the opposite number of the apparent tensile strength at an unsaturated state, σ_s represents suction stress, and σ_c is the apparent tensile strength at a saturated state and can be calculated by $\sigma_c = c'/\tan\phi'$. The variation of ϕ', ϕ_1' and ϕ_2' in Fig. 3 is so small that it can be ignored. Therefore, once the saturated Mohr-Coulomb failure envelope was obtained, the unsaturated Mohr-Coulomb failure envelope can be determined by shifting leftward the saturated Mohr-Coulomb failure envelope with a corresponding suction stress.

This study considers the effective uniaxial tensile strength of unsaturated soil calculated by an undrained triaxial test of saturated soil and how this value can truly represent the effective tensile strength of indentation test for a similar failure mode. Therefore, the effective tensile strength from the indentation test and the effective uniaxial tensile strength are compared to verify Lu's unsaturated soil mechanics framework. To obtain the effective tensile strength of the indentation test, both an indentation test and pressure plate test needed to be conducted. To determine the effective uniaxial tensile strength, consolidated undrained triaxial tests as well as pressure plate test were performed.

Experimental Programs

The indentation test uses a pair of cylindrical metal indenters to penetrate a cylindrical specimen, so the specimen must be brittle enough and can stand up by itself. Then, a large amount of sand and a little clay are required. In this study, the tested lightly cemented sand was a mixture of 85% quartz sand and 15% kaolinite by dry weight. Two different quartz sands, named RS and GS were used. RS and GS are the sand soil names and C represents the kaolinite. Therefore, the specimen named RSC represents an RS and C mixture, while GSC represents a GS and C mixture. The compositions of these two soils are detailed in Table 1. Table 2 shows the average specific gravity of these materials. The corresponding gradation curve and the Atterberg limits (ASTM 2017) are displayed in Fig. 4 (ASTM 1963) and Table 3, respectively. The silica-kaolinite mixture was considered brittle enough for the indentation test.

Two series of tests were carried out. The first series used an RSC mixture and the second series used a GSC mixture. The first series tests focused on the size effects, including the specimen height-to-diameter ratio and indenter-to-specimen-diameter ratio. In addition, the traditional and iterative method for K value were compared. For each specimen height-to-diameter ratio and indenter-to-specimen-diameter ratio, three different specimen heights were used. Before each test, the silica sand and kaolinite were well mixed with targeted water content of 8.1%. This specific moisture content was chosen to account for the plastic limit of RSC, which was 11.3%. It was found that 8.1% was quite suitable to form a test sample. The soil mixture was then stored in a sealed plastic bag cured for 24 h. The specimen was prepared by the moist tamping technique, for which a targeted dry density of 1.62 g/cm^3 was selected. The details of each indentation test configuration are presented in Table 4.

To obtain the unconfined compressive strength σ^u for the limit analysis of the indentation test, unconfined compression tests were performed following ASTM D2166 (ASTM 2016). Following ASTM D3080 (ASTM 2011b), a series of direct shear tests were conducted under normal stress of 40, 80, and 160 kPa, respectively. The direct shear testing results are modified and employed to calculate the internal friction angle, ϕ, for the limit analysis of the indentation test (Kang and Kang 2015; Kang et al. 2016a).

The second series of tests included the indentation test, unconfined compression test, direct shear test, pressure plate test (ASTM 2002), and consolidated undrained triaxial test. These tests were done to compare the effective tensile strength with two different methods to verify Lu's unsaturated framework; one is the indentation test based on limit analysis and the other one based on the unsaturated soil mechanics of Lu and Likos. The first four tests were done to determine the effective tensile strength by limit analysis, and the last two tests were conducted to get the effective uniaxial tensile strength. The dry density of the second series tests was 1.75 g/cm^3. When conducting the second series tests, specimens with three different water contents were used. Because the plastic limit of GSC was 12.2%, too high or too low moisture content would not make it possible to prepare an indentation test sample; therefore, the water contents were controlled to be 5.1%, 8.1%, 11.1%, respectively.

In the indentation tests, both the diameter and height of each specimen were kept as 100 mm. The ratio of the indenter diameter to specimen diameter was selected as 0.28. The conditions of each

Table 1. Mixing ratios

Soil type	Silica sand—RS (%)	Silica sand—GS (%)	Kaolinite—C (%)
RSC	85	0	15
GSC	0	85	15

Table 2. Average specific gravity of tested materials

Soil type	Average specific gravity
Silica sand—RS	2.66
Silica sand—GS	2.66
Kaolinite—C	2.60
RSC	2.65
GSC	2.65

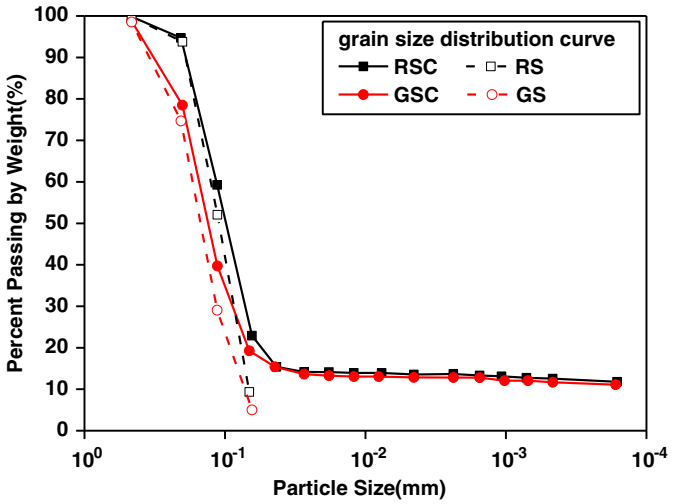

Fig. 4. Gradation curve of tested materials.

Table 3. Atterberg limits of tested soil samples

Soil type	LL (%)	PL (%)	PI (%)
RSC	13.7	11.3	2.4
GSC	14.3	12.2	2.1

Downloaded from ascelibrary.org by HUNAN UNIVERSITY on 03/20/19. Copyright ASCE. For personal use only; all rights reserved.

Table 4. Test configurations of first series indentation tests

Series	Density (g/cm^3)	Water content (%)	Specimen diameter (cm)	$H/2b$	Indenter size (cm)	a/b	Loading rate (mm/min)
RSC1	1.62	8.1	10.00	0.5	2.25	0.22	0.5
RSC2	1.62	8.1	10.00	0.5	2.81	0.28	0.5
RSC3	1.62	8.1	10.00	0.5	3.38	0.34	0.5
RSC4	1.62	8.1	10.00	1	2.25	0.22	1
RSC5	1.62	8.1	10.00	1	2.81	0.28	1
RSC6	1.62	8.1	10.00	1	3.38	0.34	1
RSC7	1.62	8.1	10.00	1.5	2.25	0.22	1.5
RSC8	1.62	8.1	10.00	1.5	2.81	0.28	1.5
RSC9	1.62	8.1	10.00	1.5	3.38	0.34	1.5
RSC10	1.62	8.1	12.00	0.5	2.81	0.23	0.6
RSC11	1.62	8.1	12.00	0.5	3.38	0.28	0.6
RSC12	1.62	8.1	12.00	0.5	4.06	0.34	0.6
RSC13	1.62	8.1	12.00	1	2.81	0.23	1.2
RSC14	1.62	8.1	12.00	1	3.38	0.28	1.2
RSC15	1.62	8.1	12.00	1	4.06	0.34	1.2
RSC16	1.62	8.1	12.00	1.5	2.81	0.23	1.8
RSC17	1.62	8.1	12.00	1.5	3.38	0.28	1.8
RSC28	1.62	8.1	12.00	1.5	4.06	0.34	1.8
RSC19	1.62	8.1	15.00	0.5	3.38	0.22	0.75
RSC20	1.62	8.1	15.00	0.5	4.06	0.27	0.75
RSC21	1.62	8.1	15.00	0.5	5.07	0.34	0.75
RSC22	1.62	8.1	15.00	1	3.38	0.22	1.5
RSC23	1.62	8.1	15.00	1	4.06	0.27	1.5
RSC24	1.62	8.1	15.00	1	5.07	0.34	1.5

Table 5. Test configurations of second series indentation tests

Series	Density (g/cm^3)	Water content (%)	Specimen diameter	$H/2b$	Indenter size	a/b	Loading rate (mm/min)
GSC	1.75	5.1	10.00	1	2.81	0.28	1
GSC	1.75	8.1	10.00	1	2.81	0.28	1
GSC	1.75	11.1	10.00	1	2.81	0.28	1

indentation test configuration are presented in Table 5. Similarly, for the limit analysis of the indentation test, unconfined compression tests, consolidated undrained tests, and a series of pressure plate tests were conducted. The pressure plate tests were conducted under normal stress of 40, 80, 160 kPa. The pressure plate tests were done following ASTM D2325 (ASTM 1968) under air pressure of 10, 20, 40, 60, 80, 120, 200, and 350 kPa. The consolidated undrained triaxial tests were conducted according to the test procedures recommended in ASTM D4767 (ASTM 2011a), while the confining pressures were controlled to be 50, 100, and 200 kPa, respectively. The water flushing technique was used to saturate the tubing and drainage system. The back-pressure saturation technique was used to saturate the specimen. Both back-pressure and cell pressure were increased simultaneously in steps of 2.5 psi. When a B value of 95% or higher was achieved, the specimen was considered to be saturated. Then, the consolidation stage started after which the specimen was sheared to failure.

ASTM D2166 (ASTM 2016) suggests that the unconfined compression test should be conducted under a loading rate ranging 0.5%–2% of axial strain per minute. From the test results presented previously (Fang and Chen 1972; Kim et al. 2007), there were no definite trends in variation of tensile strength when loading rate was changed. Kim concluded that the indentation test can be operated at the loading rate for the unconfined compression test, as recommended by ASTM standards (Kim et al. 2007). In the current study, the loading rate was chosen as 1% of axial strain per minute for both the unconfined compression test and indentation test. Data on the displacement of indenter penetration and the corresponding compressive load were recorded during the test.

Results and Discussion

Unconfined Compression Tests and Indentation Tests

Results for the unconfined compression test with three different specimen diameters are given in Fig. 5. It can be observed that the unconfined compressive strength increased as the specimen diameter increased, and less strain was needed for the specimen to reach the peak failure value. Fig. 6(a) displays the indentation test results of specimens with diameter $2b = 100$ mm broken by different indenters, and Fig. 6(b) shows the relationship of peak failure force versus specimen height-to-diameter ratio. It can be recognized from Fig. 6(a) that an increase in indenter diameter makes the peak compressive force increase and also makes it faster to reach the peak failure value. The behaviors were the same as those observed for 120-mm and 150-mm specimens indented by different indenters. A linear relationship of peak failure force and specimen height-to-diameter ratio is observed in Fig. 6(b). For the same specimen diameter, with the increase of specimen height-to-diameter ratio the peak failure force increases.

Both unconfined compressive strength and indentation force drops rapidly after achieving the peak values. For the indentation test, the specimens broke into several cone-shaped pieces at failure

Downloaded from ascelibrary.org by HUNAN UNIVERSITY on 03/20/19. Copyright ASCE. For personal use only; all rights reserved.

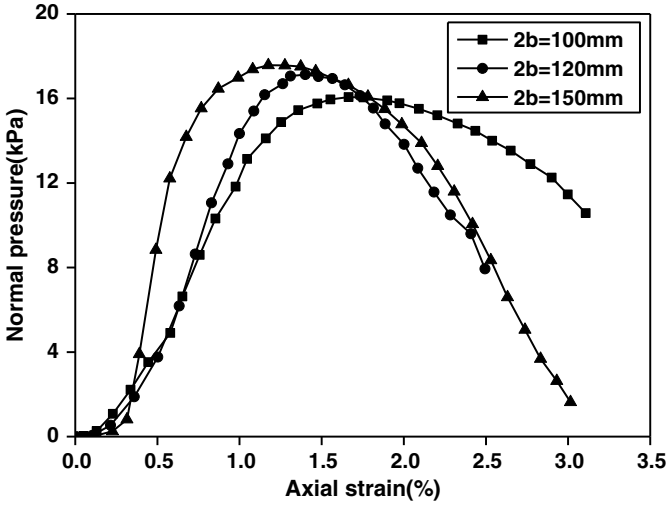

Fig. 5. Unconfined compression test of specimens with different diameters.

state, as shown in Fig. 7, indicating that the specimens all failed in a brittle mode.

Effects of Indenter Diameter to Specimen Diameter Ratios on the Tensile Strength

The influence of different a/b ratios on the tensile strength for specimens with different diameters and different specimen height-to-diameter ratios is displayed in Fig. 8. In this figure, different colored points and different symbols represent the tensile strength of different specimen sizes. It can be found that for a given a/b ratio, the tensile strengths for different specimen sizes seem concentrated in number, and the tensile strength decreases when a/b ratio increases. In general, there are no obvious relationships between tensile strength and a/b ratios for each specimen size. However, on the whole, the relationship between tensile strengths and a/b ratios can be represented by a linear equation of $\sigma^t = 1{,}350(-a/b + 1)$. In addition, for specimen diameters of 100 mm and 120 mm, the tensile strengths for different specimen size converge to a very similar value when the a/b ratio is 0.34.

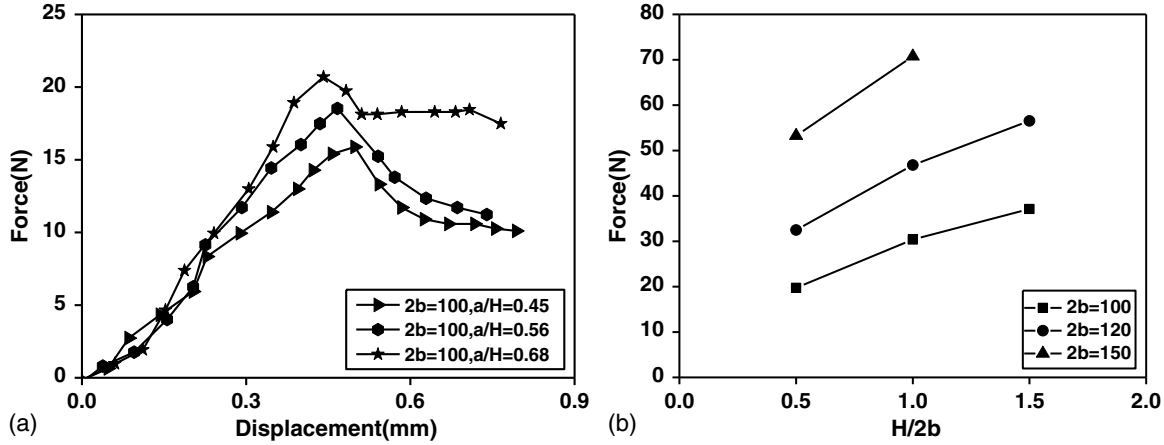

Fig. 6. Indentation test results: (a) specimens diameter $2b = 100$ mm with different indenter size; and (b) relationship of peak failure force versus specimen height-to-diameter ratios.

Fig. 7. Specimens after failure.

J. Mater. Civ. Eng., 2019, 31(1): 04018350

Downloaded from ascelibrary.org by HUNAN UNIVERSITY on 03/20/19. Copyright ASCE. For personal use only; all rights reserved.

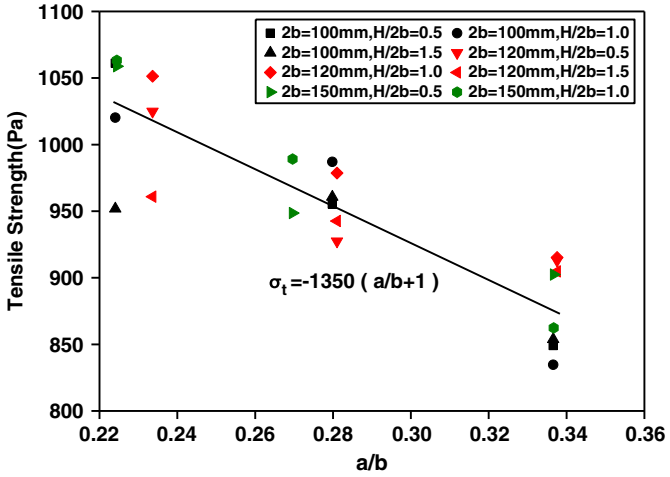

Fig. 8. Tensile strength versus a/b ratios of specimens with different $2b$ and $H/2b$ ratios.

Specimen diameter at 150 mm has the same behavior when the a/b ratio becomes 0.23.

Effects of Specimen Height-to-Diameter Ratios on the Tensile Strength

Fig. 9 illustrates the impacts of different $H/2b$ ratios on the tensile strength for specimen diameters of 100, 120, and 150 mm. The tensile strength decrease is related to the K value as shown in Eq. (5). It is speculated that larger indenter caused the larger failure cone angle α, which would amplify the K value; therefore, the tensile strength decreased. Although the relationships between tensile strengths and $H/2b$ ratios for different a/b ratios of three different specimen diameters are not explicit, it is still clear that for Figs. 9(a and b), the variation of tensile strength slightly decreased when the $H/2b$ ratio increased.

Effects of Coefficient K on the Tensile Strength

Fig. 10 compares tensile strengths obtained based on two different methods. One is the iterative method proposed in this study, and the other is the traditional method using an assumed K value (Fang and Chen 1972). The top three symbols in each figure represent results using the traditional method, while the bottom three symbols indicated results applying the iterative theory. It is found that if K is arbitrarily assumed to be 1, and K is not sensitive to ϕ and α values when brittleness is 10, the tensile strength will increase with the increase in a/b ratio and decrease in $H/2b$ ratio for specimens with diameters of 100, 120, and 150 mm. This conclusion is exactly contrary to the results obtained by the iterative method. Therefore, there was a significant difference in the tensile strength obtained by these two different methods. The tensile strength obtained by the iterative method is more concentrated and smaller than the one obtained by the traditional method; the maximum variation reached up to 2.5 times of the value obtained by iterative method.

Fig. 11 shows the relationship between the iterated K value and a/b ratio for specimens with different diameters and $H/2b$ ratios.

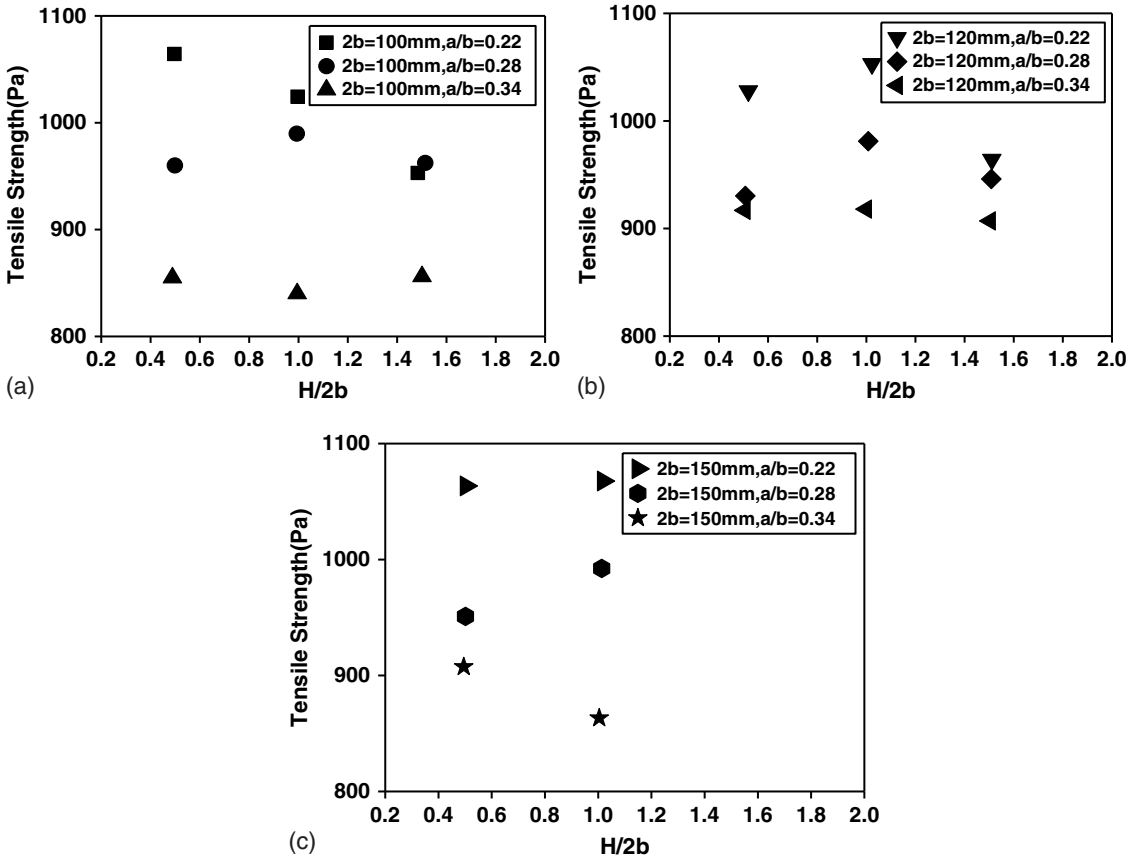

Fig. 9. Tensile strength versus $H/2b$ ratios of specimens with different $2b$ and different a/b ratios: (a) $2b = 100$ mm; (b) $2b = 120$ mm; and (c) $2b = 150$ mm.

Downloaded from ascelibrary.org by HUNAN UNIVERSITY on 03/20/19. Copyright ASCE. For personal use only; all rights reserved.

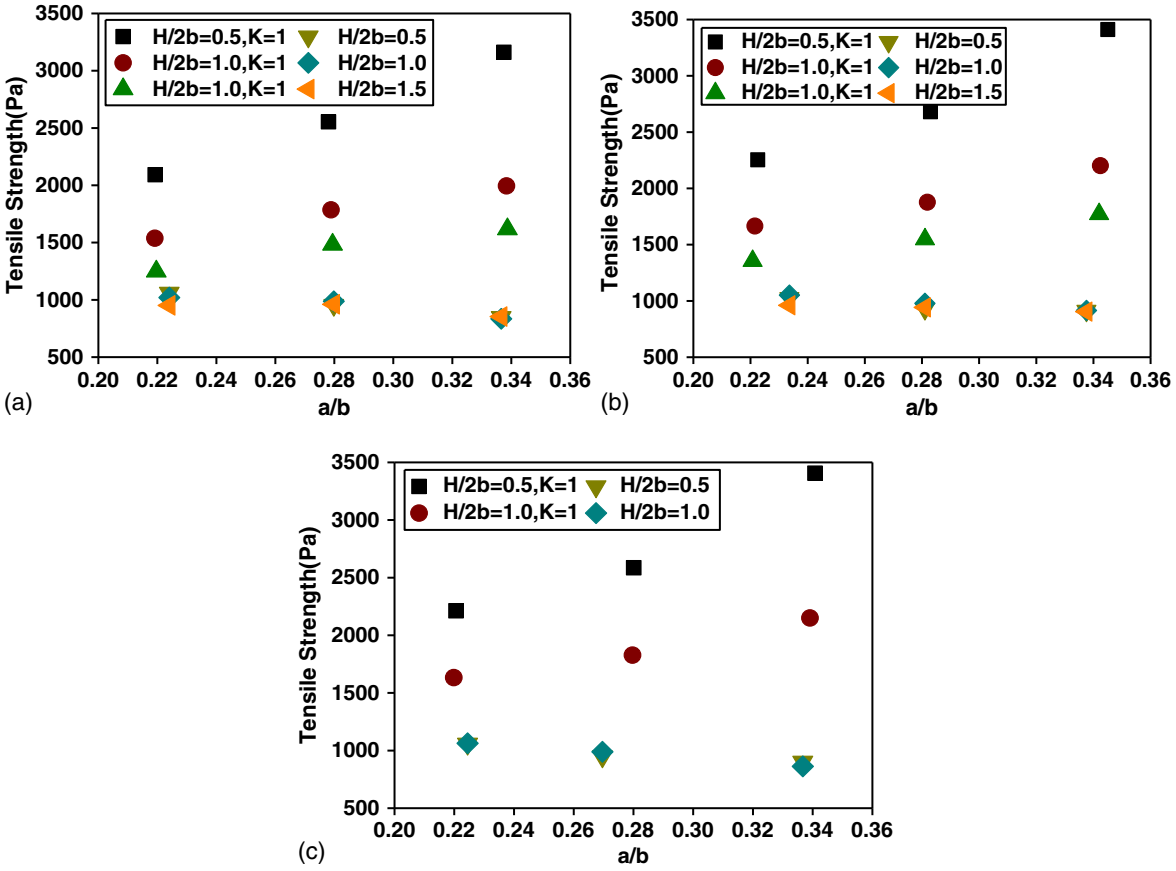

Fig. 10. Effects of coefficient K and different $H/2b$ ratios on the measured tensile strength: (a) $2b = 100$ mm; (b) $2b = 120$ mm; and (c) $2b = 150$ mm.

For a given $H/2b$ ratio, no matter how large the diameter is, the K value and a/b ratio are linearly related and can be expressed as $K = ka/b + c$. Besides, for a given a/b ratio, the K value increased with the decrease in $H/2b$ ratio; the larger the a/b ratio, the larger the K value difference. Moreover, the iterated K value in this study ranged between 1.4 and 3.5. In addition, it can be observed that the deviation of the tensile strength under different test configurations decreased for a specimen diameter of 120 mm, as shown in Fig. 12.

The first series of indentation test results are shown in Table 6. The tensile strength of lightly cemented sand is found to be dependent on specimen size and indenter size. In general, the tensile strength decreased with the increase in indenter diameter. Based on the limit analysis discussed in the previous section, the failure

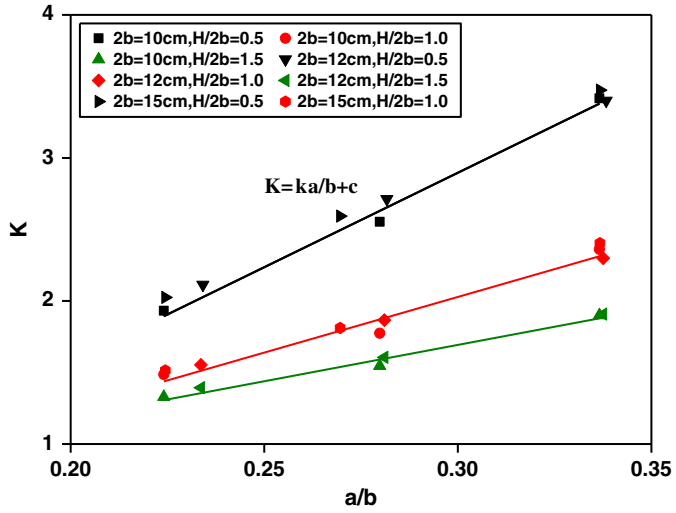

Fig. 11. Coefficient K versus a/b ratios of specimens with different $2b$ and different $H/2b$ ratios.

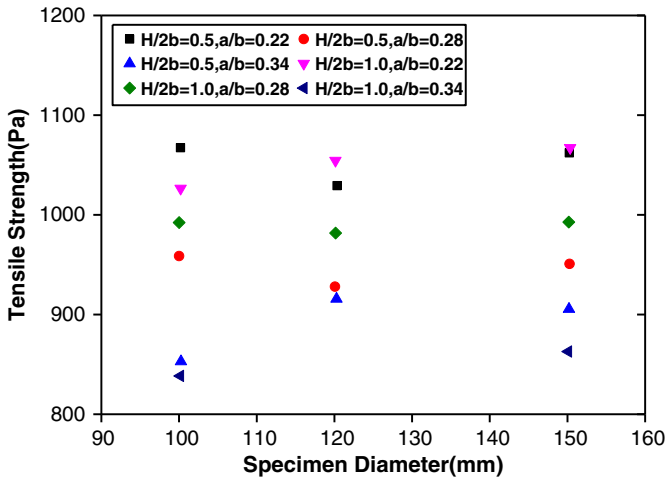

Fig. 12. Tensile strength of specimens with different $H/2b$ and a/b ratios.

Downloaded from ascelibrary.org by HUNAN UNIVERSITY on 03/20/19. Copyright ASCE. For personal use only; all rights reserved.

Table 6. Summary of first series indentation test results

b (mm)	$H/2b$ (mm)	a/b	α (degrees)	p (N)	K	σ_t (Pa)	$\sigma_{t(K=1)}$ (Pa)	σ_u/σ_t
100	0.5	0.22	15.889	16.336	1.93	1,066.44	2,111.88	15.32
100	0.5	0.28	18.871	18.531	2.55	961.07	2,577.74	17.00
100	0.5	0.34	21.405	20.695	3.41	854.98	3,179.96	19.11
100	1	0.22	12.606	23.742	1.49	1,025.14	1,535.73	15.94
100	1	0.28	15.025	28.129	1.80	992.08	1,814.14	16.47
100	1	0.34	17.974	30.710	2.33	839.16	2,024.48	19.47
100	1.5	0.22	11.096	30.130	1.33	956.19	1,275.78	17.09
100	1.5	0.28	13.131	35.065	1.55	965.31	1,506.50	16.93
100	1.5	0.34	15.696	38.442	1.90	858.10	1,660.28	19.04
120	0.5	0.22	16.912	24.580	2.11	1,028.07	2,237.70	16.91
120	0.5	0.28	19.453	28.177	2.71	930.44	2,658.64	18.68
120	0.5	0.34	21.372	34.645	3.39	916.90	3,395.93	18.96
120	1	0.22	13.187	37.161	1.55	1,053.98	1,652.75	16.49
120	1	0.28	15.483	41.807	1.87	981.39	1,865.83	17.71
120	1	0.34	17.82	47.613	2.30	918.01	2,181.58	18.93
120	1.5	0.22	11.74	45.584	1.39	963.37	1,348.70	18.04
120	1.5	0.28	13.623	51.818	1.61	945.16	1,533.19	18.39
120	1.5	0.34	15.745	58.831	1.91	907.17	1,762.75	19.16
150	0.5	0.22	16.429	37.722	2.02	1,064.03	2,210.96	16.63
150	0.5	0.28	19.022	43.412	2.59	953.84	2,589.71	18.56
150	0.5	0.34	21.532	54.965	3.47	908.19	3,436.12	19.49
150	1	0.22	12.859	57.257	1.51	1,068.08	1,631.55	16.57
150	1	0.28	15.124	63.623	1.81	993.61	1,829.65	17.81
150	1	0.34	18.28	73.434	2.40	866.62	2,155.54	20.42

cone angle α is obtained by the indenter diameter and K value, where the cone failure angle α is proportional to the indenter diameter. Therefore, a larger indenter will result in a larger crack in the specimen. K values from the iterative method fell between 1.4 and 3.5 depending on different test configurations in this study, which is quite different from the traditional K value results presented by Fang and Chen (1972). The pioneer works emphasized the importance of material properties and described that the brittle failure should minimize the failure cone angle α and lead to the specimen breaking into small pieces. According to Eq. (3) and K, the failure cone angle α dominates the magnitude of the brittleness and K value. As a result, the traditional method cannot truly present the test response, while the iterative method seems more reliable as the iterated K value closely related with different test configurations.

Unsaturated Soil Mechanics Framework on Computing Effective Tensile Strength

In Table 7, experimental results from the second series of tests compared the concept of effective tensile strength under the framework of Lu and Likos. $\sigma_{suction}$ is obtained by the pressure plate test, which means the suction stress. First, through the pressure plate test, the soil-water characteristic curve (SWCC) can be obtained, then substituting the matric suction and equivalent degree of saturation into Eq. (13), the regression equation of $\beta = 0.05$ and $n = 2.1$ can be determined. Finally, the relationship between the equivalent degree of saturation and suction stress can be obtained via Eq. (14), which is the suction stress characteristic curve (SSCC).

Table 7. Comparison of effective strength test results

w (%)	$\sigma_{suction}$ (kPa)	$\sigma_{t,up}$ (kPa)	$\sigma'_{t,up}$ (kPa)	$\sigma_{t,tri}$ (kPa)
5.1	−12.17	5.45	17.62	13.84
8.1	−16.94	0.89	17.83	17.21
11.1	−16.70	0.43	17.12	17.04

The different equivalent degrees of saturation correspond to different suction stresses, as shown in Fig. 13. $\sigma_{t,\mathrm{up}}$ represents the total tensile strength obtained by the indentation test, while $\sigma'_{t,up}$ is the effective tensile strength of indentation test, which is obtained by $\sigma_{t,\mathrm{up}}$ minus $\sigma_{suction}$. $\sigma_{t,tri}$ represents the effective tensile strength of unsaturated soil obtained by consolidated undrained triaxial tests of saturated soil and pressure plate tests. To obtain $\sigma_{t,tri}$, the Mohr-Coulomb failure envelope of saturated soil under effective confining pressures was first determined through consolidated undrained triaxial tests. Then, according to Eq. (15) and Fig. 3, the opposite number for the apparent tensile strength of unsaturated soil equals the suction stress minus apparent tensile strength of saturated soil. Therefore, the unsaturated Mohr-Coulomb failure envelope under effective confining pressure can be obtained by shifting the saturated Mohr-Coulomb failure envelope to the left by a value of suction stress selected from Fig. 13 based on the

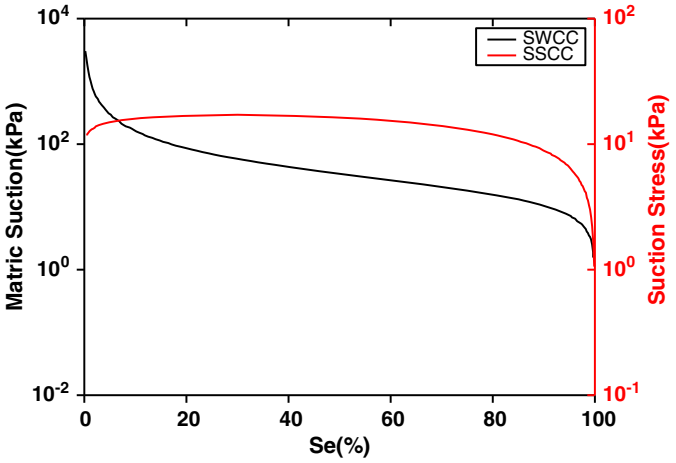

Fig. 13. Soil-water characteristic curve and suction-stress characteristic curve.

Downloaded from ascelibrary.org by HUNAN UNIVERSITY on 03/20/19. Copyright ASCE. For personal use only; all rights reserved.

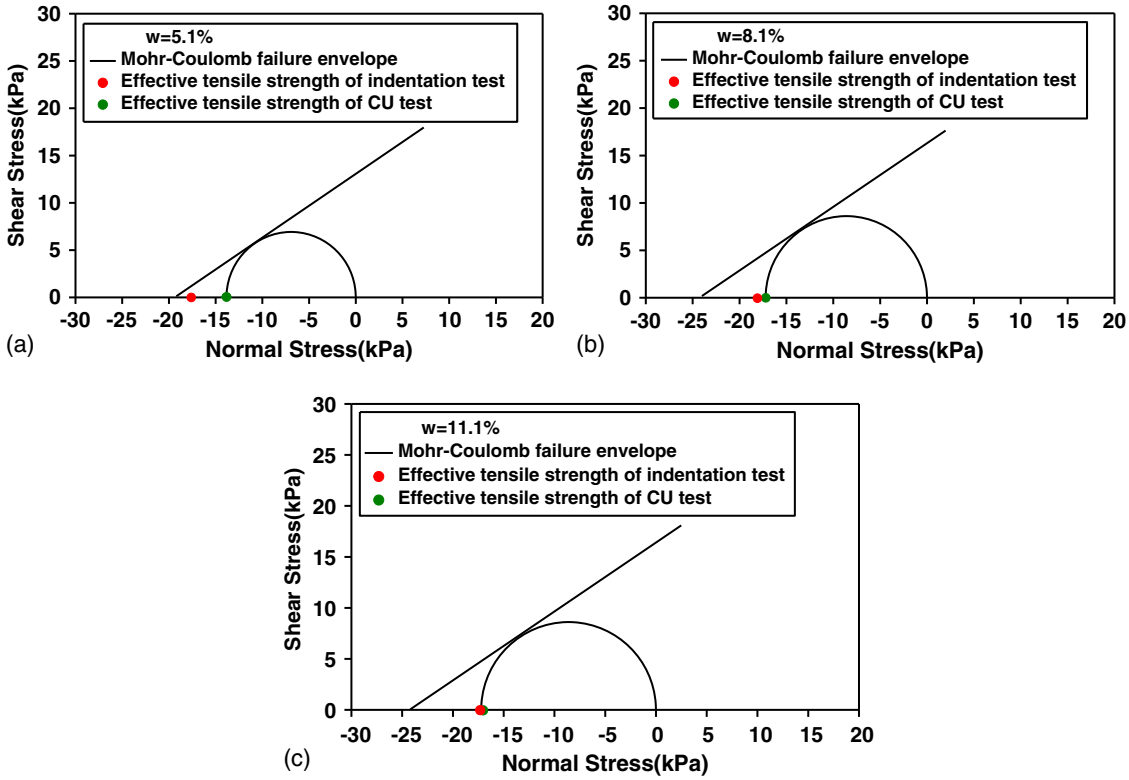

Fig. 14. Comparison of effective tensile strength at different water content w: (a) 5.1%; (b) 8.1%; and (c) 11.1%.

equivalent degree of saturation. Finally, the Mohr-circle tangent to the unsaturated Mohr-Coulomb failure envelope with maximum principle stress is set to zero and the minimum principle stress of the Mohr-circle is $\sigma_{t,tri}$.

From the results presented in Table 7, it is found that the total tensile strength, $\sigma_{t,up}$, of lightly cemented sand decreased with the increase in water content of the specimens. The value of the iterated K fell between 2 and 2.5, which is larger than the value defined by Fang and Chen (1972). On the other hand, the brittleness, σ^u/σ^t, computed as 18–25 from the testing results, also differed from the findings of Fang and Chen (1972) in which brittleness was assumed to be 10 for the compacted soil.

This study posits that the effective tensile strength of indentation test can truly describe the soil mechanics in unsaturated condition, and its value should be similar to the uniaxial tensile stress in Lu's unsaturated soil mechanics framework fora similar failure mode of the soil specimen. Fig. 14 shows the effective tensile strength values defined by the consolidated undrained triaxial test, $\sigma_{t,tri}$, and the effective tensile strength, $\sigma^f_{t,up}$, from the indentation test under the unsaturated soil mechanics framework by Lu and Likos (2006), Lu et al. (2009), and Oh et al. (2012).

To summarize the test results, it seems that the degree of saturation influences the suction stress, but has little impact on the effective tensile strength. Under the framework of suction stress, the effective tensile strengths are similar in each test configuration of the indentation test, and the variation of effective tensile strength between that of the consolidated undrained triaxial tests and that of the indentation tests was very small when the water content reached 8.1% and 11.1%. The findings showed that the application of unsaturated soil mechanic framework could perform well for the tensile strength of the lightly cemented sand using the indentation test and a certain water content.

Conclusions

In this paper, the tensile strength was determined through indentation tests. The effects of several factors, such as indenter size, specimen size, K value, and the brittleness value on the tensile strength are discussed. In general, the tensile strength is proportional to the a/b ratio and has no apparent relationship with the $H/2b$ ratio. The iterative method provides a more reliable way to compute the tensile strength beyond the traditional method. In addition, the iterated K value is linearly related to the a/b ratio for a given specimen diameter, and irrelevant to the $H/2b$ ratio value. This is likely due to the linear relationship between tensile strength and a/b ratio. In addition, the effective tensile strength obtained by the indentation test in conjunction with the pressure plate test and the consolidated undrained triaxial test are evaluated under the unsaturated soil framework. The results show that the tensile strength is very similar for certain water contents, indicating that the unsaturated soil mechanics framework is applicable in computing the tensile strength of a soil, while the unmatched portion results shows uncertainty for low water contents.

Acknowledgments

The present work was carried out with the support of the Key Laboratory of Soft Soils and Geoenvironmental Engineering (Zhejiang University), Ministry of Education (2018P03), National Key Research and Development Program of China (2016YFC0800207), National Natural Science Foundation of China (41472244), the Provincial Key Research and Development Program of Hunan Province (0105679005), the One-Thousand-Young-Talents Program of the Organization Department of the CPC Central Committee and the Hunan University Young Faculty Seed Fund.

Downloaded from ascelibrary.org by HUNAN UNIVERSITY on 03/20/19. Copyright ASCE. For personal use only; all rights reserved.

Notation

The following symbols are used in this paper:

a = radius of the indenter;
b = radius of the specimen;
c' = effective cohesion;
H = length of the specimen;
K = iterated value for limit analysis;
n = pore-size spectrum number;
P = peak axial force;
P^u = axial compressive load;
S_e = equivalent degree of saturation;
u_a = pore-air pressure;
u_w = pore-water pressure;
w = water content;
α = failure cone angle;
β = reciprocal of air-entry pressure;
σ = total stress;
σ^u = unconfined compressive strength;
σ^t = tensile strength;
σ' = effective stress of saturated soil;
σ_c = effective stress of unsaturated soil;
σ_s = suction stress of unsaturated soil;
$\sigma_{suction}$ = suction stress of indentation test;
$\sigma_{t,iso}$ = isotropic tensile strength;
$\sigma_{t,tri}$ = tensile strength defined by consolidated undrained triaxial test;
$\sigma_{t,uni}$ = uniaxial tensile strength;
$\sigma_{t,up}$ = total tensile strength of indentation test;
$\sigma_{tensile}$ = total tensile strength of indentation test;
$\sigma'_{effective}$ = effective tensile strength of indentation test;
$\sigma'_{t,up}$ = effective tensile strength of indentation test;
ϕ = internal friction angle of the soil;
ϕ' = effective angle of friction;
ϕ^b = additional angle of friction; and
χ = effective stress parameter.

References

ASTM. 1963. *Standard test method for particle-size analysis of soils*. ASTM D422. West Conshohocken, PA: ASTM.

ASTM. 1968. *Standard test method for capillary-moisture relationships for coarse- and medium-textured soils by porous-plate apparatus*. ASTM D2325. West Conshohocken, PA: ASTM.

ASTM. 2002. *Standard test methods for determination of the soil water characteristic curve for desorption using hanging column, pressure extractor, chilled mirror hygrometer, or centrifuge*. ASTM D6836. West Conshohocken, PA: ASTM.

ASTM. 2011a. *Standard test method for consolidated undrained triaxial compression test for cohesive soils*. ASTM D4767. West Conshohocken, PA: ASTM.

ASTM. 2011b. *Standard test method for direct shear test of soils under consolidated drained conditions*. ASTM D3080. West Conshohocken, PA: ASTM.

ASTM. 2016. *Standard test method for unconfined compressive strength of cohesive soil*. ASTM D2166. West Conshohocken, PA: ASTM.

ASTM. 2017. *Standard test methods for liquid limit, plastic limit, and plasticity index of soils*. ASTM D4318. West Conshohocken, PA: ASTM.

Bishop, A. W. 1959. "The principle of effective stress." *Teknisk Ukeblad* 39 (3): 859–863.

Chen, W. F. 1969. "Double punch test for tensile strength of concrete." *J. Am. Concr. Inst.* 67 (10): 993–995.

Chen, W.-F. 1975. *Limit analysis and soil plasticity*. Amsterdam, Netherlands: Elsevier.

Das, B. M., and R. N. Dass. 1995. "Lightly cemented sand in tension and compression." *Geotech. Geol. Eng.* 13 (3): 169–177. https://doi.org/10.1007/BF00456716.

Fang, H. Y., and W. F. Chen. 1972. "Further study of double punch test for tensile strength of soils." In *Proc., 3rd Southeast Asian Conf. on Soil Engineering*, 211–215.

Fang, H. Y., and J. Fernandez. 1981. "Determination of tensile strength of soils by unconfined-penetration test." *ASTM Spec. Tech. Publ.* 740 (10): 15.

Fredlund, D. G., and N. R. Morgenstern. 1977. "Stress state variables for unsaturated soils." *J. Geotech. Eng. Div.* 103 (5): 447–456.

Genuchten, M. T. V. 1980. "A closed-form equation for predicting the hydraulic conductivity of unsaturated soils." *Soil Sci. Soc. Am. J.* 44 (5): 892–898. https://doi.org/10.2136/sssaj1980.03615995004400050002x.

Kang, X., L. Ge, K.-T. Chang, and A. O. Kwok. 2016a. "Strain-controlled cyclic simple shear tests on sand with radial strain measurements." *J. Mater. Civ. Eng.* 28 (4): 0405169. https://doi.org/10.1061/(ASCE)MT.1943-5533.0001458.

Kang, X., L. Ge, and W.-C. Liao. 2016b. "Cement hydration based micromechanics modeling of the time- dependent small-strain stiffness of fly ash stabilized clayey soils." *Int. J. Geomech.* 16 (3): 04015071. https://doi.org/10.1061/(ASCE)GM.1943-5622.0000552.

Kang, X., and G.-C. Kang. 2015. "Modified monotonic simple shear tests on silica sand." *Mar. Georesour. Geotechnol.* 33 (2): 122–126. https://doi.org/10.1080/1064119X.2013.805289.

Kim, T. H., C. K. Kim, S. J. Jung, and J. H. Lee. 2007. "Tensile strength characteristics of contaminated and compacted sand-bentonite mixtures." *Environ. Geol.* 52 (4): 653–661. https://doi.org/10.1007/s00254-006-0494-8.

Kim, T. H., T. H. Kim, G. C. Kang, and L. Ge. 2012. "Factors influencing crack-induced tensile strength of compacted soil." *J. Mater. Civ. Eng.* 24 (3): 315–320. https://doi.org/10.1061/(ASCE)MT.1943-5533.0000380.

Lu, N., T. H. Kim, S. Sture, and W. J. Likos. 2009. "Tensile strength of unsaturated sand." *J. Eng. Mech.* 135 (12): 1410–1419. https://doi.org/10.1061/(ASCE)EM.1943-7889.0000054.

Lu, N., and W. J. Likos. 2006. "Suction stress characteristic curve for unsaturated soil." *J. Geotech. Geoenviron. Eng.* 132 (2): 131–142. https://doi.org/10.1061/(ASCE)1090-0241(2006)132:2(131).

Nahlawi, H., and S. Chakrabarti. 2004. "A direct tensile strength testing method for unsaturated geomaterials." *Geotech. Test. J.* 27 (4): 356–361.

Oh, S., N. Lu, K. K. Yun, S. J. Lee, and S. R. Lee. 2012. "Relationship between the soil-water characteristic curve and the suction stress characteristic curve: Experimental evidence from residual soils." *J. Geotech. Geoenviron. Eng.* 138 (1): 47–57. https://doi.org/10.1061/(ASCE)GT.1943-5606.0000564.

Tamrakar, S. B., T. Mitachi, and Y. Toyosawa. 2007. "Measurement of soil tensile strength and factors affecting its measurements." *Soils Found.* 47 (5): 911–918. https://doi.org/10.3208/sandf.47.911.

Tang, G. X., and J. Graham. 2000. "A method for testing tensile strength in unsaturated soils." *Geotech. Test. J.* 23 (3): 377–382. https://doi.org/10.1520/GTJ11059J.

Downloaded from ascelibrary.org by HUNAN UNIVERSITY on 03/20/19. Copyright ASCE. For personal use only; all rights reserved.